RSC Advances

PAPER

Cite this: *RSC Adv.*, 2023, **13**, 17179

Inkjet-printed flexible graphene paper electrode for the electrochemical determination of mercury†

Tushar Kant, [a] Kamlesh Shrivas, *[a] Tikeshwari[a] and Vellaichamy Ganesan [b]

Received 26th April 2023
Accepted 26th May 2023

DOI: 10.1039/d3ra02757k

rsc.li/rsc-advances

Here, we report an inkjet-printed graphene paper electrode (IP-GPE) for the electrochemical analysis of mercuric ions (Hg(II)) in industrial wastewater samples. Graphene (Gr) fabricated on a paper substrate was prepared by a facile solution-phase exfoliation method in which ethyl cellulose (EC) behaves as a stabilizing agent. Scanning electron microscopy (SEM) and transmission electron microscopy (TEM) were utilized to determine the shape and multiple layers of Gr. The crystalline structure and ordered lattice carbon of Gr were confirmed by X-ray diffraction (XRD) and Raman spectroscopy. The nano-ink of Gr-EC was fabricated on the paper substance *via* an inkjet printer (HP-1112) and IP-GPE was exploited as a working electrode in linear sweep voltammetry (LSV) and cyclic voltammetry (CV) for the electrochemical detection of Hg(II). The electrochemical detection is found to be diffusion-controlled illustrated by obtaining a correlation coefficient of 0.95 in CV. The present method exhibits a better linear range of 2–100 μM with a limit of detection (LOD) of 0.862 μM for the determination of Hg(II). The application of IP-GPE in electrochemical analysis shows a user-friendly, facile, and economical method for the quantitative determination of Hg(II) in municipal wastewater samples.

Introduction

Mercury (Hg) is a harmful metal pollutant that exists as Hg(II), methyl mercury (CH_3Hg), and dimethyl mercury ($(CH_3)_2$ Hg) in nature.[1] Hg is exploited in the production of cathode tubes, batteries, mercury vapor lamps, pesticides, *etc.* It is released from coal-burning industries into the ecological system.[1,2] The waste released from these industries containing Hg contaminates natural freshwater reservoirs. The entry of this toxic metal into the human body causes severe health problems including the failure of vital organs, and damage to the functions of nucleic acids and the immune system, while exposure to higher concentrations results in death.[3–5] Thus, the analysis of Hg in wastewater samples is essential to prevent contamination of clean water bodies.

There are several techniques, such as cold vapor-atomic fluorescence spectrometry (CV-AFS),[6] ICP-mass spectrometry (ICP-MS),[7] CV atomic absorption spectrometry (CV-AAS)[8] and inductively coupled plasma-atomic emission spectrometry (ICP-AES),[8] *etc.* have been available for analysis of Hg from environmental samples. Even though these techniques are highly sensitive they need expensive consumables and trained personnel for operating these sophisticated instruments. In addition, the size of these instruments is comparatively larger in size and thus it is difficult to operate at the sample source.[6–8] Thus, it is urged to develop an alternative method that should be cost-effective and portable for the determination of Hg from water samples.

Recently, nanomaterials (NMs) are exploited as sensing probes in colorimetric,[9] fluorometric,[10] electro-chemiluminescent,[11] and electrochemical[12,13] methods for analyzing Hg(II) in various samples. Amongst all these techniques, electrochemical approaches are recognized as user-friendly, inexpensive, simple, and applied at the sample source.[12] Most of the methods utilized metal NMs like platinum (Pt), gold (Au), silver (Ag), and carbon-based nanostructures.[13,14] For the preparation of NMs, expensive metallic salts such as $AgNO_3$, $HAuCl_4$, and hazardous reducing agents (such as hydrazine monohydrate, $NaBH_4$, *etc.*) are used.[14] To address this problem, carbon-based NMs such as graphene (Gr) can be an alternative material for making efficient and cost-effective electrochemical devices. Gr-based conductive nano-ink has attracted considerable attention in the electrochemical field as it shows a lowering of manufacturing cost, better stability, and better conductivity. In addition, Gr exhibits good mechanical strength and chemical stability for the fabrication of electrochemical devices.[12,15] Zhang *et al.* demonstrated a Gr-based electrochemical device for the selective study of Hg(II). Here, the glassy carbon electrode (GCE) modified with Gr and DNA was applied for sensing Hg(II) in drinking water by differential pulse voltammetry (DPV).[16] Motlagh *et al.* illustrated the modification of GCE with Gr and methacrylic acid polymer and exploited it for the measurement

[a]*School of Studies in Chemistry, Pt. Ravishankar Shukla University, Raipur-492010, C.G., India. E-mail: kshrivas@gmail.com*

[b]*Department of Chemistry, Institute of Science, Banaras Hindu University, Varanasi-221005, UP, India*

† Electronic supplementary information (ESI) available. See DOI: https://doi.org/10.1039/d3ra02757k

of Hg(II) in water samples.[17] However, modified GCE with NMs showed excellent electrocatalytic properties for Hg(II) detection but the major disadvantage is the tedious and time-consuming process of casting the functional materials on the GCE surface.[18] The successful deposition of NMs on GCEs is a challenging job and there is a possibility of disruption of the electrode surface during the electrochemical analysis. Therefore, simple and rapid fabrication techniques such as direct writing,[19] spin coating,[20] screen printing,[21] and inkjet printing[22] are used for the deposition of NMs on solid substrates (photo paper, plastic, glass, ceramics, *etc.*). Among these, inkjet printing is a convenient, quick, and cost-effective method for fabricating NMs on flexible surfaces.[14] Our group reported the fabrication of Gr-EC on photo paper *via* inkjet printer and further applied as a working electrode (WE) for H_2O_2 detection.[15] Thus, the utilization of paper-based printed electrodes in electroanalytical measurements demonstrated user-friendly, excellent stability, and low cost.

In the present work, Gr-based nano-ink has been prepared *via* solution-phase exfoliation method. Herein, graphite powder is taken as a precursor, and ethyl cellulose (EC) acts as a stabilizer, separately. The synthesized Gr-EC was dissolved in an appropriate solvent to prepare nano-ink and then printed on photo paper by an inkjet printer. The inkjet-printed graphene paper electrode (IP-GPE) has been used as a WE for the determination of Hg(II). Finally, IP-GPE was applied as an electrochemical sensing platform for analyzing Hg(II) in industrial wastewater samples using LSV.

Experimental section

Materials

All of the reagents and chemicals utilized in this study are of AR quality. Graphite flakes were obtained from Sigma Aldrich (MA, USA). Ethyl cellulose, disodium hydrogen phosphate (Na_2HPO_4), cyclohexanone, and terpineol were obtained from TCI Chemicals Pvt. Ltd (Chennai, India). Mercuric chloride ($HgCl_2$) and sodium dihydrogen phosphate (NaH_2PO_4) were purchased from HiMedia Laboratories Pvt Ltd (Mumbai, India). The phosphate buffers (7.0–9.0 pH) were prepared using solutions of NaH_2PO_4 and Na_2HPO_4.

Synthesis of Gr-EC

The Gr was synthesized by direct exfoliation of graphite powder using an ultrasonication process with some modifications described in the previous work.[23,24] Briefly, 2 g of graphite powder was taken into a 250 mL flask containing 50 mL of ethyl alcohol and 2% (w/v) EC. The solution was sonicated for 1.5 h and the obtained product was centrifuged at around 10 000 rpm for 15 min. Further, the black precipitate acquired from centrifugation was kept at room temperature for drying. After that, the material was dispersed into ethanol and then filtered through a syringe filter (5 μm sieve) to eliminate the larger-sized particles. Further, it was washed with distilled water 3–4 times, and finally, the black precipitate was dehydrated at 50 °C in an oven to get the fine particles of Gr-EC.

Synthesis of Gr-EC nano-ink and IP-GPE

Herein, Gr-EC black powder was dispersed in cyclohexanone and terpineol for inkjet printing. The prepared nano-ink was sonicated and filtered to remove any large particles, which might block the printer cartridge during the printing process. The pre-cleaned cartridge of HP-1112 was filled with 2 wt% Gr-EC nano-ink with the help of a micropipette and then the electrode-like structure of dimensions (length 6 cm, breadth 0.2 cm with 1 cm^2 area at the lower part) was printed on a paper substrate (Scheme 1). The IP-GPE was sintered for about 30 min at 200 °C to make an efficient electrode for electrochemical detection.

Sample collection from industrial wastewater for the analysis of Hg(II)

The samples from industrial wastewater were collected into 100 mL bottles in the month of December 2021 from Raipur City, Chhattisgarh, India, using the prescribed procedures.[18] All the collected wastewater samples were filtered and stored under 5 °C for further analysis.

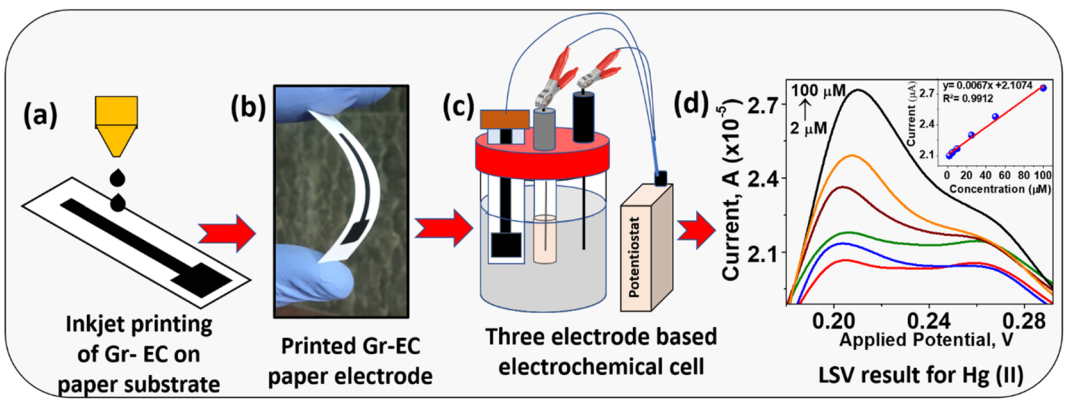

Scheme 1 Diagrammatic representation of (a) inkjet printing of Gr-EC on a paper substrate, (b) flexible inkjet-printed graphene paper electrode, (c) electrochemical cell containing three electrodes for Hg(II) detection, and (d) LSV peaks for different concentrations of Hg(II).

Instrumentation

UV-Vis spectrophotometer (Evolution-300, Thermo Scientific) was used to measure the localized surface plasmon resonance (LSPR) absorption band of Gr-EC. The crystalline structure of Gr was measured by the Bruker D8-Focus diffractometer in the 2θ range of 10°–80° at a sweep rate of 0.5° min^{-1}. The functional group of Gr with EC was investigated by Fourier transform-infrared (FT-IR) Type ALPHA II, Bruker. The stability of Gr-EC was estimated by thermal gravimetric analysis (TGA, 8000, PerkinElmer) in the range of 25–600 °C. The morphology of Gr-EC was characterized by transmission electron microscopy (TEM Tecnai G2S-Twin, Philips) and field emission scanning electron microscopy (FE-SEM, JSM-7000F). The elemental constitution was confirmed by X-ray photoelectron spectroscopy (XPS) Type (PHI 5000 Versa Probe III, Physical Electronics). The average height and average roughness of the Gr nanosheets were calculated by scanning probe microscope including atomic force microscopy (AFM, NT-MDT-INTEGRA). Laser micro Raman analysis was studied with Jobin Yvon Labram-010, in the 632.8 nm wavelength with a 1 μm^2 spot size.

Procedure for Hg(II) detection using IP-GPE in CV and LSV

The IP-GPE was employed as WE while Ag/AgCl and Pt wire as the reference electrode (RE) and counter electrode (CE), correspondingly in CV and LSV for detection of Hg(II). CV and LSV measurements were performed to measure the concentration of Hg(II) in 0.1 M phosphate buffer scanning in the potential window from −0.1 to 0.5 V with a 100 mV s^{-1} sweep rate. The quantitative determination of Hg(II) was carried out by spiking different concentrations of Hg(II) from 2 to 100 μM and the calibration curve was drawn based on the reduction peak current to estimate Hg(II) present in the industrial wastewater samples.

Result and discussion

Characterization

UV-Vis spectroscopy study was initially utilized to characterize the synthesis of Gr sheets and the localized surface plasmon absorption band at 265 nm in Fig. 1(a) indicates the existence of C–C conjugated aromatic ring due to the of π–π* electronic transition.[15] Fig. 1(b) illustrates the crystal structure of the Gr layer with (001), (002), (101), and (004) planes at different angles of diffraction. The characteristic peak observed at $2\theta = 22.4°$ is similar to the peak observed for graphite having the uniform structure with diverse layers and spacing of 0.341 nm.[25] Therefore, the interplanar distance of Gr is a little higher than the graphite, mostly due to the deformed structure of graphite.[16,25]

The stabilization of different functional groups on the Gr surfaces was identified using FTIR spectroscopy. The FTIR data of EC and Gr-EC are shown in Fig. 1(c), indicating a broad peak at 3340 cm^{-1} due to strong OH stretching in Gr-EC.[17] The presence of dual peaks detected at 2973 and 2879 cm^{-1} exhibiting the C–H stretching indicates the dispersion of EC on Gr sheets. The appearance of a low-intensity peak at 657 cm^{-1} of Gr indicates the confirmation of the C=C double bond which is absent in EC. A medium intense peak that appeared at 1378 cm^{-1} is attributed to the CH_3 bending from EC. Two sharp intense peaks were observed at 1044 and 1084 cm^{-1} for C–O–C

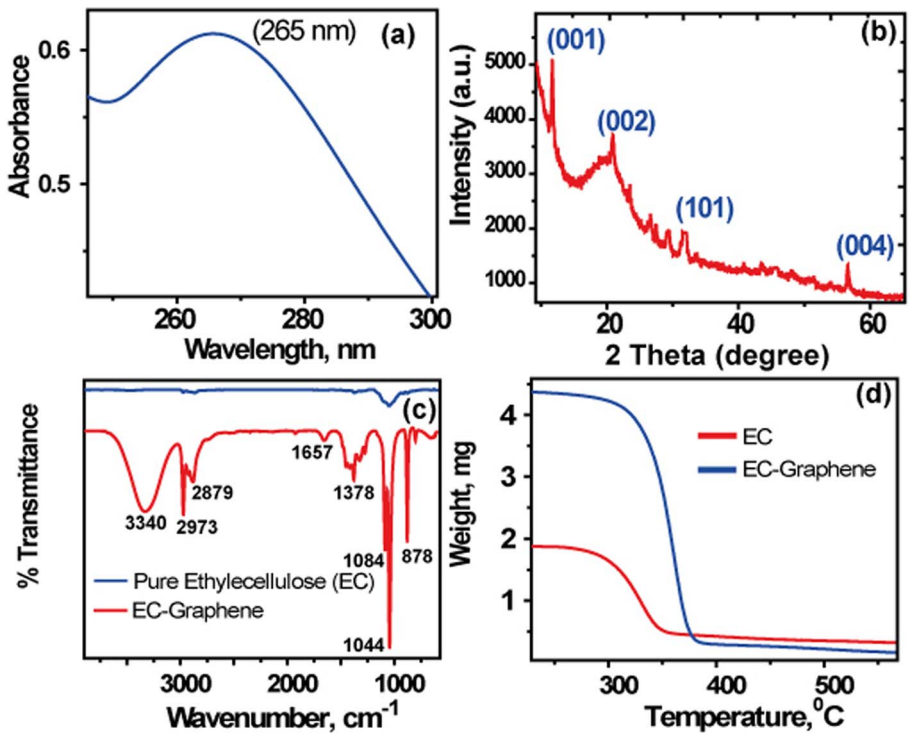

Fig. 1 (a) UV-vis absorbance spectra, (b) XRD pattern, (c) FTIR spectra, and (d) TGA curve for Gr-EC.

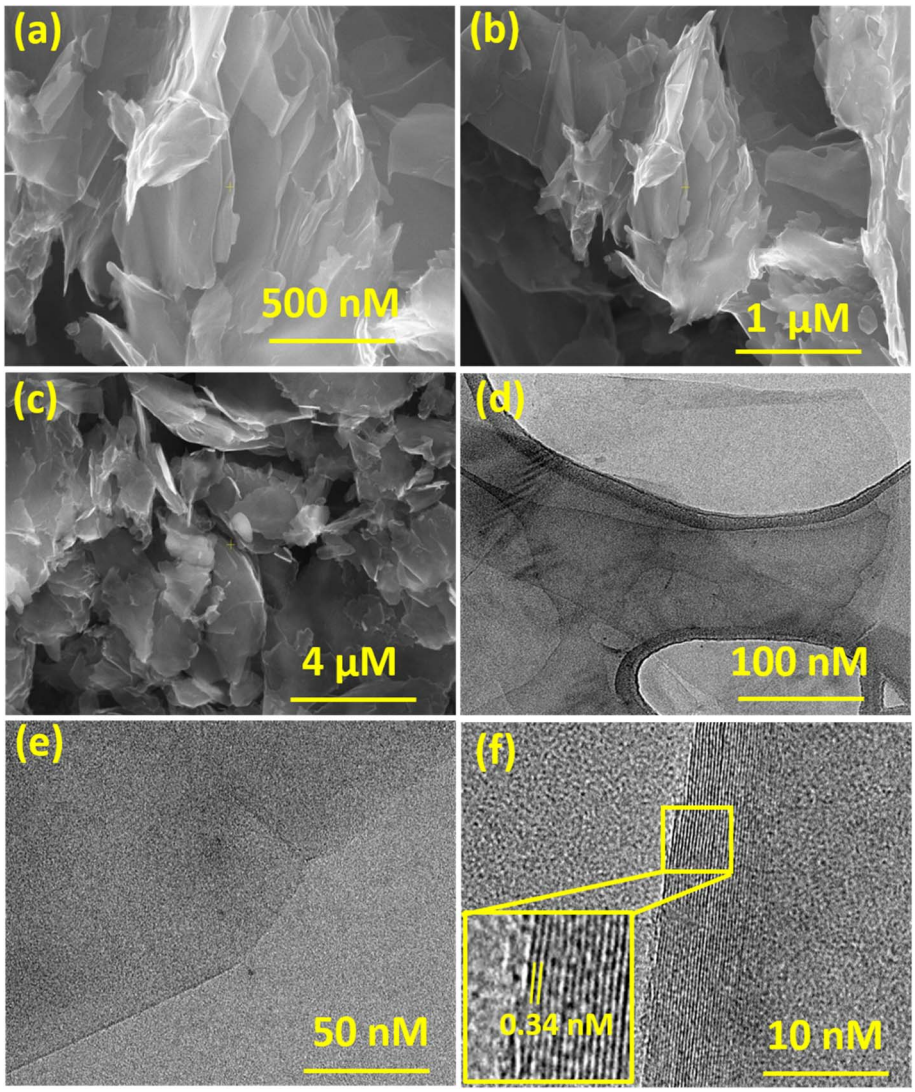

Fig. 2 (a)–(c) SEM images of Gr-EC and (d)–(f) TEM images of Gr-EC.

stretching from EC.[15,16,25] Further, TGA has been applied to find out the stability in the synthesized Gr-EC (Fig. 1(d)). The result shows that stability in the heat of Gr is increased with stabilizing with EC molecules. The Gr-EC showed decomposition at 320 °C compared to EC at 300 °C.[24]

The morphological structure of synthesized Gr-EC has been confirmed by SEM and TEM analysis given in Fig. 2(a to d). The Gr image shows a thin flat flake with a crumpled shape, which is consistent with prior results.[26] The wrinkled flake structure resembled the thin film morphology Gr sheets. The two-dimensional sheet structure confirmed by TEM (HR-TEM) is shown in Fig. 2(e). This shows a good view of the image (Fig. 2(f)) to reveal that the Gr has multiple layers with the *d*-spacing value calculated to be 0.34 nm.[15,26]

The imperfections and disorder of the carbon framework are examined by Raman analysis shown in Fig. 3(a). Different characteristic peaks that appeared at 1369, 1592, and 2851 cm^{-1} are allocated to D, G, and 2D bands, correspondingly of Gr-EC.[27] These bands are generated as a result of disordered (A_1g symmetry), graphitic (E_2G symmetry), and overtone (2D bands) respectively. A good strength of the G band in Gr-EC indicates the well-ordered sp^2 carbon framework demonstrating the exfoliated Gr. However, the D band revealed imperfection as well as a disorder which are directly accomplished through the disarrangement of sp^2 carbon.[16,27] I_D/I_G is the ratio of relative intensity relation of D and G bands Gr-EC (0.16) showed ordered lattice carbon is present in Gr-EC which showed negligible defects in both edge and basal planes of Gr. These confirmed that Gr-EC contains the crystal lattice of Gr *via* EC exfoliation process. This process converted the graphite powder into Gr-sheets in different layers.[23,27] Additionally, oxygen-containing functional groups have also been introduced here for stabilization with EC. Therefore, EC supported the exfoliation process *via* sonication breakdowns of the van der Waals force found in graphite, and the exfoliation process convert graphite into Gr sheets.[15,26] The chemical states and bonding of carbon and oxygen in Gr-EC are exemplified by XPS. The XPS spectrum of Gr-EC is shown in Fig. 3(b–d). Surveys of XPS containing C 1s

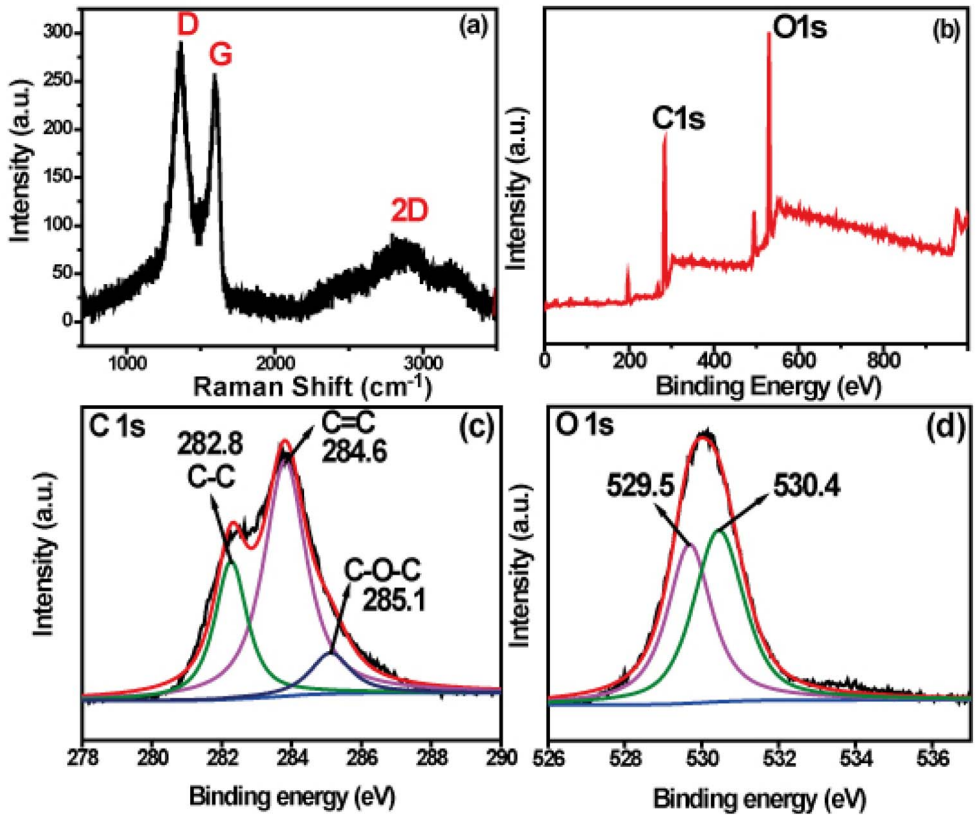

Fig. 3 (a) Raman spectrum (b) XPS survey spectrum, (c) C 1s spectrum and (d) O 1s spectrum of Gr-EC.

and O 1s peaks are shown in Fig. 3(b). The resolution band of C in 1s shows intense peaks at 285.1 eV for C–O–C and 282.8 eV for C–C bonds. Similarly, the intensive peaks are observed for C–O–C and C–C at 285.1 and 282.8 eV, respectively when the band obtained for C 1s is resolved (Fig. 3(c)). The appearance of peaks is credited to oxygen functionalities of Gr-EC from EC polymer as well as sp^2 graphitic carbon, individually.[27] Furthermore, the spectra of 1s O are shown in Fig. 3(d) to indicate the presence of two peaks placed at 530.4 and 529.5 eV for and O–C=O and C–O correspondingly.[27] In addition, imaging of the surface structure of Gr-EC has been done using AFM. Fig. S1† shows the typical height of fabricated Gr-EC, which appears to be about 274.22 nm while the average roughness of the nanosheet is observed as 95.93 nm (Table S1†).

Optimization of Gr-EC and IP-GPE for electrochemical application

Several parameters such as the selection of paper substrate, the selection of solvents for ink preparation, surface tension and viscosity of nano ink, number of printing layers, sintering time and temperature, *etc.* were optimized to obtain effective and efficient IP-GPE for electrochemical application. All parameters were optimized in previous research work.[15] In summary, the stable and uniform distribution of Gr in a solvent was prepared that did not aggregate even after a long period of storage. For this, different organic solvents were taken into account for optimization, and found that the solvent mixture of cyclohexanone and terpineol exhibits a high degree of dispersion of Gr-EC. A 2 wt% Gr-EC in the solvent mixture showed better stability with 35 mN M^{-1} surface tension and 12 mPa s viscosity. Further, an inkjet printer was employed to print the nano-ink on various paper substrates and photo paper showed better results with homogenous distribution of Gr due to the small pore size of the paper substrate. For improvement of conductivity and electrochemical application, the prepared IP-GPE was sintered at different temperature with several time intervals and found that 200 °C for 30 min were sufficient.

Electrodes behavior comparison with bare GCE and IP-GPE for Hg(II)

IP-GPE was taken as a WE for electroanalytical sensing of Hg(II) by CV. To know electrochemical sensing ability, the current density of IP-GPE (surface area 1 cm^2) against bare GCE (surface area 0.071 cm^2) (pH 4.5) was calculated by analysis of 250 μM Hg(II) in 0.1 M PBS. Fig. 4(a) shows a cyclic voltammogram plotted between current density and potential. It is clear that the IP-GPE exhibits better current density than bare GCE because NMs have a larger surface area and fast electron transfer reaction for the electrochemical reduction of Hg(II) to Hg(0). In addition, the use of PBS solution affected the determination of Hg(II) by CV, shown in Fig. 4(b).Therefore, IP-GPE was employed as an electrochemical sensing platform for the analysis of Hg(II) from the sample solution.

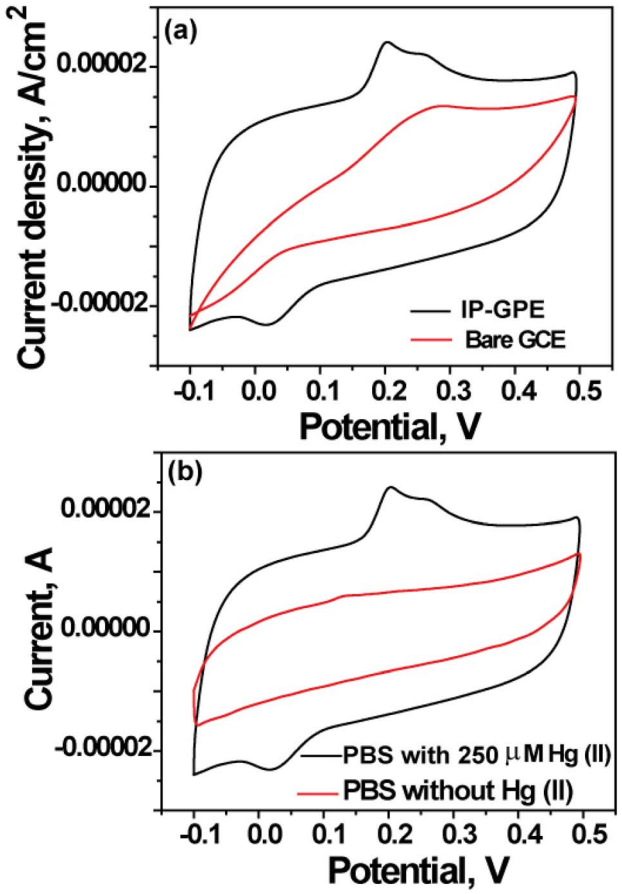

Fig. 4 (a) CV results of (a) bare GCE on taking the IP-GPE as working electrode for sensing of 250 μM Hg(II) in 0.1 M PBS (pH 4.5) at 100 mV s^{-1} sweep rate; (b) IP-GPE when used as a WE in 0.1 M PBS (pH 4.5) with and without Hg(II) at 100 mV s^{-1} scan rate.

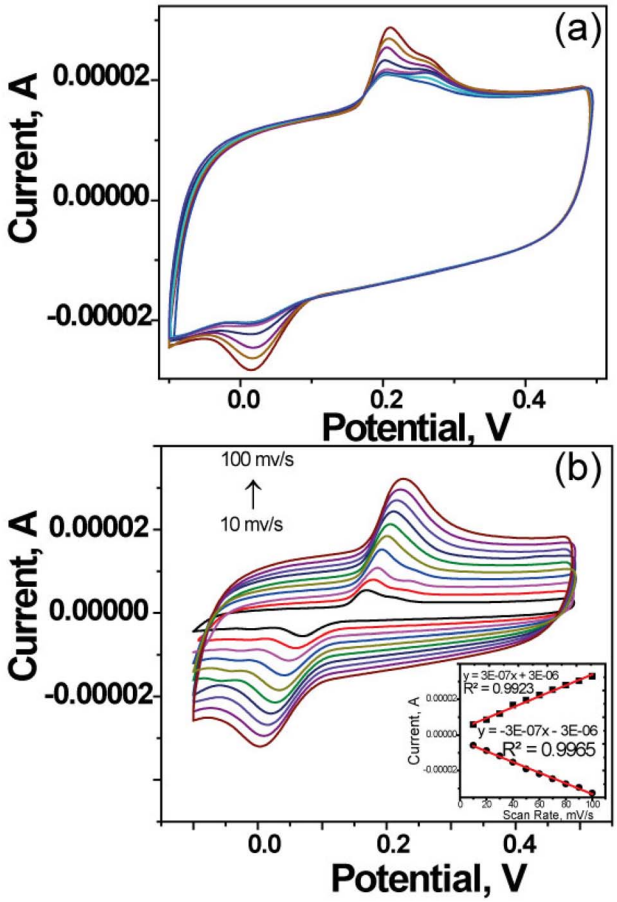

Fig. 5 (a) CV response of Hg(II) from 0.1 mM to 1 mM concentration using IP-GPE in 0.1 M PBS (pH 4.5) at a sweep rate of 100 mV s^{-1} and (b) CV of 1 mM Hg(II) at IP-GPE at several sweep rates from 10 to 100 mV s^{-1}.

Electrochemical approach for detection of Hg(II) using IP-GPE in CV

The electrode performance of IP-GPE was examined for the analysis of Hg(II) using CV in a wide linear range from 100 to 1000 μM. The results are displayed in Fig. 5(a). The redox current peak is observed when the potential varies from −0.10 V to 0.50 V. The transport of electrons between IP-GPE and Hg(II) solution is found to be relatively slow. Two reduction peaks for Hg(II) are observed at 0.22 V and 0.28 V. The reduction of mercury started at ∼0.2 V, which is in respectable agreement with the previously reported values.[28] The following is the mechanism for the reduction process.

$$Hg^{2+} + e^- \rightarrow Hg^+ \quad (1)$$

$$Hg^+ + e^- \rightarrow Hg^0 \quad (2)$$

Fig. 5(a) shows multiple CV peaks at different concentrations (2 to 100 μM) of Hg(II) using IP-GPE as a WE. The anodic peak current (−2.05 μA) at 0.019 V is observed when we scan negative to positive potential which is a slow process. Further, in the

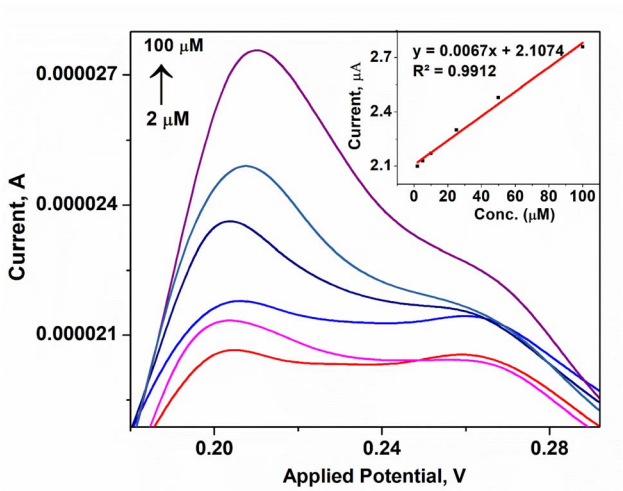

Fig. 6 LSV plots of Hg(II) from 2 to 100 μM concentrations using IP-GPE in 0.1 M PBS (pH 4.5) at a 100 mV s^{-1} sweep rate and calibration curve in the inset.

Table 1 Analytical study of Hg(II) in industrial wastewater samples using IP-GPE in LSV

Sample sources	Hg(II), μM	RSD, %
Urla, Raipur	3.2	1.7
Siltara, Raipur	4.1	1.9
Birganw, Raipur	3.5	1.2
Bhanpuri, Raipur	3.3	1.8
Tatibandh, Raipur	ND	—
Mandhar, Raipur	ND	—

second cycle, two reduction peaks with current 2.17 and 2.05 μA at 0.2 and 0.25 V were observed, respectively. Further, the reduction peak current obtained at 0.2 V is considered for analysis of Hg(II). To investigate the nature of the electron transfer process between IP-GPE and solution, various scan rates from 10 to 100 mV s^{-1} were investigated. Fig. 5(b) demonstrates the effect of sweep rates on the peak current of Hg(II). It is observed that the peak current is improved as the potential is shifted from 0.07 to 0.0 V. Furthermore, the linear relation among peak current as well as sweep rate is designated using the equation: $I_{pa} = -3 \times 10^{-7}$ to -3×10^{-6}. The correlation coefficient is observed to be 0.9965 indicating the electrode process is diffusion controlled.

Analytical study for determination of Hg(II) in LSV

Several analytical parameters, including linearity range, the limit of detection (LOD), precision, and accuracy were estimated to determine Hg(II) using LSV. For this, LSV peaks of Hg(II) were recorded with a linear increase in the concentration beginning from 2 to 100 μM in phosphate buffer (0.1 M). It is seen that the peak current is increased with increasing Hg(II) concentration, shown in Fig. 6. A linear line is observed for different concentrations of Hg(II) with a good correlation coefficient of 0.991. The LOD was computed based on the three times the standard deviation of the blank and divided by the slope value from the calibration curve. This has been applied to describe the minimum value of the targeted analyte which could be measured during the analytical process. The LOD for Hg(II) in LSV was observed to be 0.862 μM.

Next, fabricated IP-GPE was exploited as a WE for measurement of 50 μM Hg(II) in phosphate buffer for consecutive 30 days (Fig. S2 and Table S2†). From the result, there is no significant change in LSV curves for prescribed periods showing the stability of electrodes that can be used for multiple analyses. Further, the precision of the method was calculated in terms of relative standard deviation percentage (%) by considering the standard deviation of the reduction peak current of 30 cycles. The % RSD acquired for determination of Hg(II) was 3.02% to demonstrate the fabricated electrode has satisfactory reproducibility (Table S3†).

Application of the IP-GPE for sensing of Hg(II) in industrial wastewater

The real applicability of IP-GPE was employed in LSV for Hg(II) determination in industrial water samples. Herein, different water samples were analyzed in LSV at the optimized conditions of the method. The obtained reduction peak current of samples is considered for calculating the concentration of Hg(II) using standard calibration curves. The result is summarized in Table 1. Additionally, the recovery percentage was calculated to know the selectivity of the method in the presence of complex sample matrices. For this, different concentrations of Hg(II) (8 and 10 μM) were added to the collected industrial water sample (target analyte not detected), and recovery% was calculated. The obtained results showed better performance of IP-GPE towards Hg(II) detection with a recovery percentage of 94–95% demonstrating the selectivity of the electrode (Table S4†). Further, IP-GPE was employed for the analysis of Hg(II) in the presence of 250 mgL^{-1} of Cr(III), Fe(III), Fe(II), Cu(II), and Pb(II), and 500 mgL^{-1} of NO_2^-, NO_3^-, SO_4^{2-} and Cl^-that might existed in water samples. For this, different ions were added containing Hg(II), there are no additional peaks observed in the LSV indicating the selectivity of the present methodology.

Comparison for determination of Hg(II) using IP-GPE/LSV to other electrochemical methods

The performance of IP-GPE is compared with other Gr-based nanomaterials (NMs) such as polyglycine-modified Gr paste electrode (PGMGPE),[28] ultrafine tin oxide/rGO (SnO_2/rGO),[29]

Table 2 Comparison of IP-GPE for determination of Hg(II) by electrochemical method with other graphene-based NMs

NMs based electrode	Technique	Linear range	LOD	R^2	Samples	Ref.
PGMGPE	CV	100–1000 μM	6.6 μM	0.99	Water and blood serum	28
SnO_2/rGO	SWASVs	0.4–1.2 μM	12.2 nM	0.984	Drinking water	29
GO/MCH/PTO/gold	CV	1–300 nM	1 nM	0.982	—	30
rGO/–SH/Au-NPs	DPV	1–10 μM	0.2 μM	0.972	Tap water	31
GO/Au/GCE	SWV	10–100 nM	0.01 nM	0.983	River water	32
ZnO/rGO/PPy	DPV	2–18 nM	1.9 nM	0.995	Seawater	33
PEDOT/GO/GCE	DPSV	10–10^3 nm	2.78 nM	—	Tap water	34
rGO/CeO_2/GCE	DPASV	0.02–2.5 μM	23.4 nM	0.998	Waste water	35
DNA-RGO	DPVs	8–100 nM	5 nM	0.996	River water	36
AuNPs/GO-IL GCE	ASV/DPV	0.1–100 nM	0.03 nM	0.980	Drinking water	37
Gr-βCD/Ppy/SPCE	DPV	1–51nM	0.47 nM	—	—	38
IP-GPE	LSV	2–100 μM	0.862 μM	0.996	Industrial waste water	Present work

graphene oxide/6-mercapto-1-hexanol/gold (GO/MCH/PTO/gold),[30] rGO/dodecanethiol/AuNPs(rGO/–SH/Au-NPs),[31] GO/Au/GCE,[32] zinc oxide/rGO/polypyrrole (ZnO/rGO/PPy),[33] poly(3,4-ethylene dioxythiophene) nanorods/GO/GCE (PEDOT/GO/GCE),[34] rGO/cerium oxide/GCE (rGO/CeO_2/GCE),[35] DNA-rGO (DNA-rGO)[36] ionic liquid GO (GO-IL),[37] AuNPs/GO-IL-GCE[38] and Ppy-GO/β-cyclodextrin (Gr-βCD/Ppy/SPCE)[38] for determination of Hg(II) by CV, LSV, SWV, and DPV, *etc.* (Table 2). Most of the electrochemical methods showed better sensitivity compared to IP-GPE/LSV. However, most of these reported methods used lengthy steps for the synthesis of graphene and the casting process for the fabrication of Gr-based NMs on GCE which is extensive and tedious. The main limitation of IP-GPE/LSV is the lower sensitivity compared to other reported methods. However, the IP-GPE/LSV is applicable where the concentration of the target analyte would be in higher concentration in the range of 2–100 μM.

Conclusions

In summary, the fabrication of inkjet-printed graphene paper-based paper electrodes is low-cost, eco-, and user-friendly, and can be produced on a large scale for electrochemical applications. In addition, the graphene was synthesized by a simple exfoliation process without the use of lengthy steps and toxic chemicals. IP-GPE was successfully employed as an electrochemical sensing platform for the determination of Hg(II) in municipal wastewater samples. The IP-GPE exhibited better selectivity and recovery% for the determination of target analyte in the presence of other chemicals. The limitation of this method is low sensitivity for analysis of Hg(II) which will be improved in the near future. The advantages of employing IP-GPE in CV and LSV are low cost, flexible, and simple for the determination of Hg(II) in several environmental samples.

Conflicts of interest

There are no conflicts to declare.

Acknowledgements

Science and Engineering Research Board (SERB), New Delhi is acknowledged for providing financial assistance in the form of Extra Mural Research Project (File No: EMR/2016/005813) to Kamlesh Shrivas. Vellaichamy Ganesan thanks the IoE grant of BHU (scheme number 6031) for financial support.

References

1 K. Yoshizawa, E. B. Rimm, J. S. Morris, V. L. Spate, C. C. Hsieh, D. Spiegelman, M. J. Stampfer and W. C. Willett, *N. Engl. J. Med.*, 2002, **347**, 1755–1760.
2 F. Zahir, S. J. Rizwi, S. K. Haq and R. H. Khan, *Environ. Toxicol. Pharmacol.*, 2005, **20**, 351–360.
3 S. Ekino, M. Susa, T. Ninomiya, K. Imamura and T. Kitamura, *J. Neurol. Sci.*, 2007, **262**, 131–144.
4 P. Chakraborty, *Sci. Total Environ.*, 2017, **589**, 232–235.
5 Z. Sahebi, Md. R. M. Shafiee and M. Emtyazjoo, *Adv. Environ. Biol.*, 2011, **5**, 920–928.
6 P. R. Aranda, R. A. Gil, S. Moyano, I. De Vito and L. D. Martinez, *J. Hazard. Mater.*, 2009, **161**, 1399–1403.
7 J. Allibone, E. Fatemian and P. J. Walker, *J. Anal. At. Spectrom.*, 1999, **14**, 235–239.
8 G. Jarzynska and J. Falandysz, *J. Environ. Sci. Health*, 2011, **46**, 569–573.
9 Monisha, K. Shrivas, T. Kant, S. Patel, R. Devi, N. S. Dahariya, S. Pervez, M. K. Deb, M. K. Rai and J. Rai, *J. Hazard. Mater.*, 2021, **414**, 125440.
10 C. K. Chiang, C. C. Huang, C. W. Liu and H. T. Chang, *Anal. Chem.*, 2008, **80**, 3716–3721.
11 B. Babamiri, A. Salimi and R. Hallaj, *Biosens. Bioelectron.*, 2018, **102**, 328–335.
12 H. Park, S. J. Hwang and K. Kim, *Electrochem. commun.*, 2012, **24**, 100–103.
13 T. Kant, K. Shrivas, K. Tapadia, R. Devi, V. Ganesan and M. K. Deb, *New J. Chem.*, 2021, **45**, 8297.
14 K. Shrivas, A. Ghosale, P. K. Bajpai, T. Kant, K. Dewangan and R. Shankar, *Microchem. J.*, 2020, **156**, 104944.
15 T. Kant, K. Shrivas, I. Karbhal, Monisha, S. Yadav, Tikeshwari, S. Sahu, Y. K. Mahipal and V. Ganesan, *New J. Chem.*, 2022, **46**, 1362–1370.
16 Y. Zhang, H. Zhao, Z. Wu, Y. Xue, X. Zhang, Y. He, X. Li and Z. Yuan, *Biosens. Bioelectron.*, 2013, **48**, 180–187.
17 M. G. Motlagh, M. A. Taher, A. Heydari, R. G. Motlagh and V. K. Gupta, *Mater. Sci. Eng., C*, 2016, **63**, 367–375.
18 O. Abollino, A. Giacomino, M. Malandrino, G. Piscionieri and E. Mentasti, *Electroanalysis*, 2008, **20**, 75–83.
19 A. Ghosale, K. Shrivas, R. Shankar and V. Ganesan, *Anal. Chem.*, 2017, **89**, 776–782.
20 M. B. Sahana, C. Sudakar, C. Thapa, G. Lawes, V. M. Naik, R. J. Baird, G. W. Auner, R. Naik and K. R. Padmanabhan, *Mater. Sci. Eng., B*, 2007, **143**, 42–50.
21 A. Ghosale, K. Shrivas, M. K. Deb, V. Ganesan, I. Karbhal, P. K. Bajpai and R. Shankar, *Anal. Methods*, 2018, **10**, 3248–3255.
22 T. Kant, K. Shrivas, V. Ganesan, Y. K. Mahipal, R. Devi, M. K. Deb and R. Shankar, *Microchem. J.*, 2020, **155**, 104687.
23 S. D. Amaya, L. K. Lin, R. E. DiNino, C. Ostos and L. A. Stanciu, *Electrochim. Acta*, 2019, **316**, 33–42.
24 E. B. Secor, P. L. Prabhumirashi, K. Puntambekar, M. L. Geier and M. C. Hersam, *J. Phys. Chem. Lett.*, 2013, **4**, 1347–1351.
25 K. K. Khichar, S. B. Dangi, V. Dhayal, U. Kumar, S. Z. Hashmi, V. Sadhu, B. L. Choudhary, S. Kumar, S. Kaya, A. E. Kuznetsov, S. Dalela, S. K. Gupta and P. A. Alvi, *Polym. Compos.*, 2020, **41**, 1–11.
26 X. Huang, Z. Yin, S. Wu, X. Qi, Q. He, Q. Zhang, Q. Yan, F. Boey and H. Zhang, *Small*, 2011, **7**, 1876–1902.
27 A. Yamuna, P. Sundaresan and S. M. Chen, *Ultrason. Sonochem.*, 2019, **59**, 104720.
28 C. Raril and J. G. Manjunatha, *J. Anal. Sci. Technol.*, 2020, **11**, 2738.
29 Y. Wei, C. Gao, F. Meng, H. H. Li, L. Wang, J. H. Liu and X. Jiu Huang, *J. Phys. Chem. C*, 2012, **116**, 1034–1041.

30 H. Park, S. J. Hwang and K. Kim, *Electrochem. Commun.*, 2012, **24**, 100–103.
31 N. R. Devi, M. Sasidharan and A. K. Sundramoorthy, *J. Electrochem. Soc.*, 2018, **165**, B3046–B3053.
32 Y. Zhang, G. M. Zeng, L. Tang, J. Chen, Y. Zhu, X. X. He and Y. He, *Anal. Chem.*, 2015, **87**, 989–996.
33 Y. Zhuang, M. Zhao, Y. He, F. Cheng and S. Chen, *J. Electroanal. Chem.*, 2018, **826**, 90–95.
34 Y. Zuo, J. Xu, X. Zhu, X. Duan, L. Lu, Y. Gao, H. Xing, T. Yang, G. Ye and Y. Yu, *Synth. Met.*, 2016, **220**, 14–19.
35 Y. L. Xie, S. Q. Zhao, H. L. Ye, J. Y. P. Song and S. Q. Hu, *J. Electroanal. Chem.*, 2015, **757**, 235–242.
36 Y. Zhang, H. Zhao, Z. Wu, Y. Xue, X. Zhang, Y. He, X. Li and Z. Yuan, *Biosens. Bioelectron.*, 2013, **48**, 180–187.
37 N. Zhou, J. Li, H. Chen, C. Liao, Z. Chen and L. Chen, *Analyst*, 2013, **138**, 1091–1097.
38 S. Palanisamy, K. Thangavelu, S. M. Chena, V. Velusamy, I. H. Chang, T. W. Chen, F. M. A. Hemaid, M. A. Ali and S. K. Ramaraj, *Sens. Actuators, B*, 2017, **243**, 888–894.